Phase Reshaping via All-Pass Filters for Robust LCL-Filter Active Damping

Yao, WenLi; Yang, Yongheng; Xu, Yan; Blaabjerg, Frede; Liu, Shuyong; Wilson, Gary

Published in:
I E E E Transactions on Power Electronics

DOI (link to publication from Publisher):
10.1109/TPEL.2019.2927272

Publication date:
2020

Document Version
Accepted author manuscript, peer reviewed version

Phase Reshaping via All-Pass Filters for Robust LCL-Filter Active Damping

Wenli Yao, *Member*, *IEEE*, Yongheng Yang, *Senior Member*, *IEEE*, Yan Xu, *Senior Member*, *IEEE*, Frede Blaabjerg, *Fellow*, *IEEE*, Shuyong Liu, and Gary Wilson

***Abstract* — Active damping is a common way to stabilize the current control of *LCL*-filtered converters. In this paper, the stable region of −180°-phase-crossing is firstly identified within a predefined range of grid impedance and *LCL* parameter variations. Once the phase of the current control loop is in the identified region, a stabilization control can be attained. Subsequently, digital filters can be adopted to achieve active damping by reshaping the open-loop phase. Various digital filters are selected and benchmarked in this paper. It is confirmed that the all-pass filter has a unity gain and adjustable lagging phase before the Nyquist frequency, thereby being a promising solution to the phase reshaping. Therefore, the all-pass filter is employed to move the phase of the open-loop control (i.e., −180°-phase crossing) into the targeted region for active damping. Notably, the current controller and the all-pass filter-based active damping can be separately designed, indicating the easy implementation of the active damping. Experimental tests demonstrate that the proposed method can ensure the system stability over a wide range of parameter variations (e.g., grid impedance changes and *LCL*-filter parameter drifts) while maintaining fast dynamics with the grid-side current control.**

***Index Terms* – All-pass filter, active damping, *LCL* filter, digital control, parameter variations, PWM converters.**

I. INTRODUCTION

LCL-filtered single-phase AC/DC converters are commonly used in grid-connected applications [1], [2]. As a third-order system, the resonant peak of the *LCL* filter may challenge the system stability, depending on the controlled current (i.e., the converter-side current or the grid-side current), switching frequency and delay in the control loop [3]-[5]. In [3], it has been revealed that if an one-step delay (z^{-1}) is considered in a digital control loop, a critical frequency f_{cri} being 1/6 of the switching frequency f_s can be identified. It has been further indicated that damping is necessary for the grid-side current feedback (GCF) control if the resonant frequency f_{res} is lower than the critical frequency (i.e., $f_{res} < f_{cri}$). On the other hand, for the converter-side current feedback (CCF) control, the damping is mandatory if $f_{res} > f_{cri}$. To ensure a general stable operation, either "passive" or "active" damping is required for such systems. The passive damping usually needs power-dissipation elements, which inevitably incurs additional power losses [6]. In contrast, the "active" method only modifies the control algorithm without extra passive components, and thus being commonly adopted in many *LCL*-filtered inverters for damping [7].

In fact, most of the "active" methods adopt the online impedance estimation, either a single-loop or multi-loop feedback control to realize the damping [8]-[28]. The multi-loop feedback methods introduce an additional damping term into the denominator of the open-loop transfer function to mimic the characteristics of a passive damping resistor or impedance, known as virtual resistance or virtual impedance methods. Typically, the virtual resistor is realized by feeding the capacitor current into the control loop [8], [9]. For instance, a high-pass filter [8] and a delay compensation [9] were employed to improve the active damping performance. The capacitor voltage feedback is an alternative that can provide the capacitor current [10]-[12], and however, it requires a complicated algorithm (e.g., the second-order generalized integrator – SOGI [11] and a lead-lag filter [12]) to differentiate the capacitor voltage into its current. Other solutions like the Lyapunov-function-based method was proposed in [13] by using both inductor currents to achieve stable operation. However, requiring additional sensors is the major drawback of multi-loop feedback methods. In addition, the controller design of multi-loop methods is relatively complicated.

To simplify the system and then achieve cost-effective damping, online impedance estimation and single-loop control methods are recommended. The online impedance estimation is realized by injecting perturbation signals, e.g., binary sequences [14] and pseudo random sequences [15], into the system, and then the response is measured and sent to the estimation algorithm to calculate the grid impedance. Subsequently, the control algorithm can be adaptively modified to maintain the stability. However, the online grid impedance measurement requires complicated algorithms [14]-[17] and/or hard-

Manuscript received December 16, 2018; revised March 23, 2019 and May 15, 2019; accepted June 25, 2019. This is the peer-reviewed version of a paper accepted by IEEE TRANSACTIONS ON POWER ELECTRONICS. Date of final submission July 4, 2019. Recommended for publication by Associate Editor X. XX. *(Corresponding author: Yan Xu.)*

W. Yao is with the Rolls-Royce@NTU Corporate Lab, School of Electrical and Electronics Engineering, Nanayang Technological University, 639798, Singapore, and also with the School of Automation, Northwestern Polytechnical University, Xi'an 710072, China (e-mail: yaowl@nwpu.edu.cn).

Y. Xu is with the School of Electrical and Electronic Engineering, Nanyang Technological University, Singapore 639798 (e-mail: xuyan@ntu.edu.sg).

Y. Yang and F. Blaabjerg are with the Department of Energy Technology, Aalborg University, Aalborg 9220, Denmark (e-mail: yoy@et.aau.dk; fbl@et.aau.dk).

Shuyong Liu and Gary Wilson are with Electrical Capability Group of Rolls-Royce Singapore. (e-mail: Gary.Wilson5@Rolls-Royce.com and Shuyong.Liu@Rolls-Royce.com).

Color versions of one or more of the figures in this paper are available online at http://ieeexplore.ieee.org.

Digital Object Identifier 10.1109/TPEL.2019.xxxxxxx

ware modifications [17]. Moreover, the accuracy of the estimation is critically important for the damping performance [7]. Alternatively, active methods employing digital filters [18]-[23], virtual impedances in parallel with the filter inductor [24], state observers [25], and impedance reshaping [26], [27] are single-loop-control representatives. For example, in [24], the grid current was fed forward to the current control loop, enabling adequate damping of the resonance without additional measurements. Among those, the impedance reshaping method recently gains much attention [26], [27]. Reshaping the input impedance via voltage feedforward can achieve a pre-designed stability margin. Inserting a digital filter into the current controller becomes intuitive to "filter" the resonance of the *LCL*-filter, being the filter-based solution [18]-[23]. However, as mentioned in [23], the control bandwidth will be compromised.

Notably, the aforementioned methods are normally coupled with the controller design. In order to achieve high control bandwidth and simplify the design procedure, it is straightforward to only reshape the open-loop phase for the stability enhancement. By doing so, the current controller and active damping design can be separated into two independent stages. In [5], it has been mentioned that by changing the sampling start instant and the CMP loading time, a non-integer unit time delay can be introduced to reshape the phase-frequency curve. This is simple, but it may suffer from aliasing errors and in turn affect the performance of the grid current control [8], [9]. Moreover, it will make the delay time not be integer times of the unit delay z^{-1}, and thus it may require a complicated discretization of the delay transfer function in the control implementation. Considering this, the phase reshaping with all-pass filters is one of the most promising solutions, since the all-pass filter features a unity gain in the entire frequency range. The simplest all-pass filter z^{-n} (n is an integer) was recommended in [5] to change the critical frequency f_{cri}, but its fixed lagging phase limits the phase reshaping flexibility. In [21], the all-pass filter (AF) was introduced to guarantee zero phase at the resonance frequency f_{res}. However, the tolerance of the grid impedance L_{g} and *LCL* filter parameter variations is uncontrollable, since such variations are not considered during the design phase. In addition, as the phase of the *LCL*-filter at f_{res} is highly related to the equivalence series resistor (ESR) of the inductor and capacitor, the ESR may bring additional issues when choosing the lagging phase of the AF.

In this paper, a novel AF design strategy is thus proposed to ensure the system stability of the GCF control. The controller is designed systematically considering a certain variation range of the *LCL*-filter parameters and grid impedance. Firstly, the current controller is designed to ensure desired bandwidth f_{b} for the system. Then, with the pre-defined variation range of the *LCL*-filter parameters and grid impedance, a stable region can be obtained, where the open-loop gain is always below 0 dB. This indicates that, once the −180º-phase-crossing of the open-loop system is reshaped into the identified region, a stable system is achieved. Therefore, the final step of the proposed method is to design the lagging phase of the AF to move the −180º-phase-crossing point into the identified stable region, rather than reshaping the open-loop phase to zero at f_{res}, as presented in [21]. In the proposed method, only one coefficient related to the AF phase should be determined. As an extended study of [22], this paper also demonstrates that the effect of the ESR on the crossover frequencies is relatively small, and then, the system open-loop gain can be simplified. Here, the Cardano's method is employed to find the solution. Furthermore, applying the AF to the CCF control is also explored in this paper. It has been identified that the step-up of a 180º-phase change at the anti-resonant frequency ($f_{\text{at-res}}$) may introduce another −180º-phase-crossing between $f_{\text{at-res}}$ and f_{res}, which may complicate the design.

The rest of this paper is organized as follows. In § II, the system control structure of the *LCL*-filtered converter is introduced, followed by an analysis of the crossover frequency to identify the stable region. § III gives an overall comparison of the digital filters that can be employed for phase reshaping. The tuning procedure of the AF for the GCF control is discussed in § IV, where the robustness analysis of the entire closed-loop current control considering parameter variations is also presented. The limitation of the AF when applied to the CCF control is explained in § V. Experimental results are provided in § VI to verify the proposed active damping design method. Finally, concluding remarks are provided in § VII.

II. SYSTEM DESCRIPTION AND SAFETY REGION IDENTIFICATION

Fig. 1 shows a grid-connected single-phase AC/DC converter with an *LCL* filter, where C_{f} is the filter capacitor, L_1 and L_2 are the converter side inductor and the grid side inductor, respectively. Moreover, r_1, r_2, and r_{d} can be considered as the ESRs of the filter inductors and capacitor. The grid voltage v_{g} is measured for synchronization, and L_{grid} represents the grid impedance under a weak grid condition. The *LCL* filter parameters are given in Table I. Normally, both the grid-side current (i_2: GCF) and converter-side current (i_1: CCF) can be fed back to the inner current loop. The GCF control is more convenient for the control of active power and passive power. Hence, the GCF control is adopted in this paper. Considering the grid impedance, the transfer function of the *LCL* filter in the s-domain from the converter output voltage v_{con} to the grid current i_2 can be given as

$$G_{\text{i2}}(s)=\frac{i_2(s)}{v_{\text{con}}(s)}=\frac{n_1 s+1}{d_3 s^3+d_2 s^2+d_1 s+d_0} \tag{1}$$

where $d_0 = r_1+r_2$, $d_1 = L_1+L_{\text{g}}+C_{\text{f}}\cdot(r_{\text{d}}r_2+r_{\text{d}}r_1+r_1r_2)$, $d_2 = C_{\text{f}}\cdot[L_{\text{g}}\cdot(r_{\text{d}}+r_1) + L_1\cdot(r_{\text{d}}+r_2)]$, $d_3 = C_{\text{f}}\cdot L_{\text{g}}\cdot L_1$, and $n_1 = C_{\text{f}}\cdot(r_{\text{d}}+r_2)$. Moreover, $L_{\text{g}} = L_{\text{grid}} + L_2$ representing the total grid-side inductance. The resonant frequency can be calculated as

$$\omega_{\text{res}}=\sqrt{\frac{1}{C_{\text{f}}}\cdot\left(\frac{1}{L_1}+\frac{1}{L_{\text{g}}}\right)}=\sqrt{\frac{L_1+L_{\text{g}}}{L_1L_{\text{g}}C_{\text{f}}}} \tag{2}$$

in which $\omega_{\text{res}} = 2\pi f_{\text{res}}$ being the resonant angular frequency of the *LCL* filter.

A. Traditional current controller design and stability problem

The overall control structure for the single-phase AC/DC converter is depicted in Fig. 2 with an outer DC voltage control loop and an inner grid current control loop. The grid voltage is fed to a phase-locked loop (PLL) for synchronization. As seen, the outer control path is to regulate the DC output

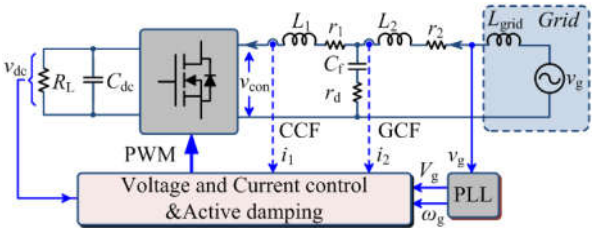

Fig. 1. Grid-connected single-phase AC/DC converter with an *LCL* filter (PLL: Phase-locked loop).

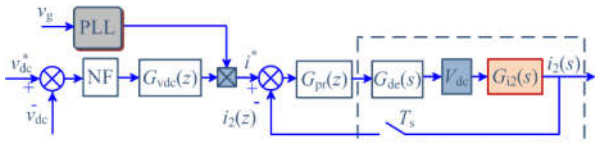

Fig. 2. Closed-loop current control system using the grid current feedback (GCF) for the single-phase AC/DC converter with an *LCL* filter.

TABLE I.
PARAMETERS OF THE SINGLE-PHASE AC/DC CONVERTER.

Converter Side Inductor	L_1 =1.8 mH
Grid Side Inductor	L_2 = 1. 1mH
Filter Capacitor (GCF)	C_f = 15 uF
Filter Capacitor (CCF)	C_f = 2.5 uF
Grid Impedance	L_{grid} = 0~10 mH
Sampling Frequency	f_s = 10 kHz
Grid Voltage	V_g = 110 V/50 Hz
DC Bus Voltage	V_{dc} = 225 V

voltage v_{dc} to follow a constant reference v_{dc}^* [29]. Moreover, the DC output voltage v_{dc} is filtered by a notch filter (NF) tuned at twice the fundamental grid frequency to remove the second-order ripple voltages. Then, a proportional-integral (PI) controller is employed to control the DC output voltage. The output of the PI controller is multiplied by a grid-synchronized sinusoidal signal, giving the inner current reference i^*. Finally, a quasi-proportional-resonant (quasi-PR) controller is adopted to regulate the grid current to follow the reference [33]. Using the Tustin transformation with pre-wrap to discretize the quasi-PR controller results in

$$G_{pr}(z)=K_p+\left\{\frac{K_p\omega_c\sin(\omega_0T_s)(z^2-1)}{T_r}\cdot \frac{1}{\left[\omega_0+\omega_{PR}\sin(\omega_0T_s)\right]z^2-2\omega_0\cos(\omega_0T_s)z+\left[\omega_0-\omega_{PR}\sin(\omega_0T_s)\right]}\right\} \quad (3)$$

where K_p and T_r are the controller parameters, T_s is the sampling period, ω_{PR} is the cutoff frequency, and ω_0 is the fundamental grid frequency. The cutoff frequency ω_{PR} can be set appropriately to tolerate possible grid frequency variations (e.g., ±2% of the rated). In addition, K_p can be tuned according to the optimized relationship between K_p and the control bandwidth ω_b by appointing a desired phase margin ϕ_m (e.g., ϕ_m = 60°) [3], and T_r can be calculated by ensuring that its phase contribution is small at the crossover frequency, thus leading to

$$K_p=\frac{\omega_b(L_1+L_2)}{V_{dc}},\qquad T_r=\frac{\tan(\phi_m+\omega_bT_d)}{\omega_b} \quad (4)$$

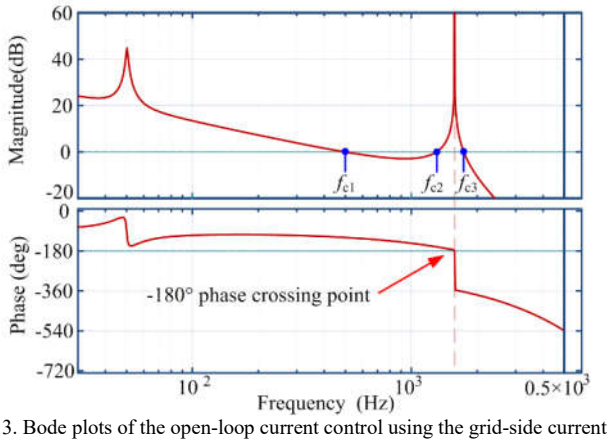

Fig. 3. Bode plots of the open-loop current control using the grid-side current feedback without active damping.

in which T_d is the total delay in the control loop. The sampling and computation process can be accounted as a time delay of T_s [4], and the total delay can then be given as $G_{de}(s) = e^{-sT_d} = e^{-1.5sT_s}$, as shown in Fig. 2. In general, the DC voltage control is much slower than the inner current loop. Hence, it can be assumed that the voltage control has negligible impact on the current control. Then, only the stability of the inner loop is considered [29]. According to Fig. 2, the open-loop transfer function of the GCF control can be expressed in the *z*-domain as [4]

$$G_{open}(z)=Z\{G_{open}(s)\}=G_{pr}(z)\cdot Z\{G_{de}(s)\cdot V_{dc}\cdot G_{i2}(s)\} \quad (5)$$

Notably, the Zero-Order-Hold (ZOH) transform can be employed to discretize the open-loop transfer function in (5). With the converter parameters listed in Table I, Fig. 3 shows the Bode plot of the discretized $G_{open}(z)$. As shown in Fig. 3, in the frequency range with the magnitude above 0 dB, the phase-response has a negative crossing of the −180°-phase (denoted as $N_- = 1$) and there are no positive crossings (represented by $N_+ = 0$), resulting in $N_+ - N_- \neq 0$. *A*ccording to the Nyquist stability criterion [4], there are unstable poles in the open-loop system. If the negative crossing N_- can be avoided by employing the active damping with the proper reshaping of magnitude- or phase-responses, the system stability can be guaranteed. This is the concept of the reshaping active damping. Normally, reshaping the magnitude-response makes the active damping be coupled with the controller design, possibly leading to reduced control bandwidth. In the conventional way, this is undesired in certain applications. In those cases, it is expected to decouple the stability of resonant controllers from the influence of the *LCL* resonance, where the highest order of harmonics that can be compensated is usually constrained by the control bandwidth [4], [35]. Even if this constraint can be extended to be beyond the control bandwidth by adopting the resonant controller with detailed phase compensation, the active damping is still coupled with the controller design. Thus, in order to simplify the design, the phase reshaping is employed in this paper for the stability enhancement.

B. Identification of stable region for −180°-phase crossing placement

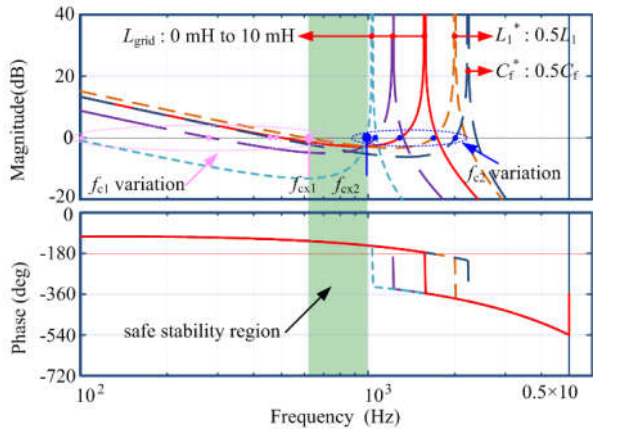

Fig. 4. Bode plot of the open-loop system with different *LCL* filter parameter and grid impedance L_{grid}.

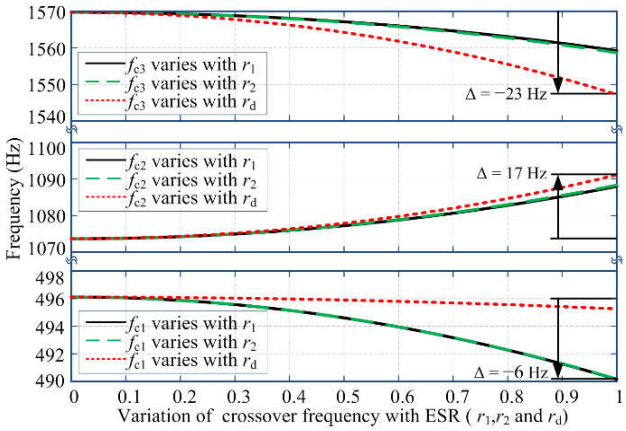

Fig. 5. Variation of the crossover frequency f_{c1}, f_{c2} and f_{c3} with different ESRs (r_1, r_2 or r_d).

According to Fig. 3, the GCF control has two regions with negative gains. One is between the crossover frequencies f_{c1} and f_{c2}; the other is between f_{c3} and the Nyquist frequency. Hence, the −180°-phase-crossing point can be reshaped to one of the two negative gain regions to reduce the negative crossing N_-. The high-frequency region (between f_{c3} and the Nyquist frequency) is not desired, as it requires large leading phase to compensate. That is, placing the −180°-phase-crossing point between f_{c1} and f_{c2} is recommended. Moreover, f_{c1} and f_{c2} may change with the grid impedance L_{grid} and *LCL* -filter parameters, and clearly, it is necessary to explore how f_{c1} and f_{c2} move with the parameter variations in order to find the optimal −180°-phase-crossing point. It is assumed that the variations of the parameters are in a pre-defined range, e.g., L_{grid} being 0 to 10 mH and the drift of the filter capacitance and inductance being up to 50%. With this, Fig. 4 shows how the magnitude and phase of the open-loop system change accordingly. Referring to Fig. 4, f_{c2} is always larger than f_{c1} under different parameters. The smallest f_{c2} is obtained in the case of the largest grid impedance (i.e., L_{grid} = 10 mH), denoted as f_{cx2}. On the other hand, the largest crossover frequency f_{c1} is related to the 50%-decrease of the converter side inductor L_1 and it is represented as f_{cx1}. Thus, between f_{cx1} and f_{cx2}, the magnitude of the open-loop is always below 0 dB. This means that in the predefined parameter variation range, once the −180°-phase-crossing point is assigned to be between f_{cx1} and f_{cx2}, the stability of the current control can be ensured. Hence, the frequency range from f_{cx1} to f_{cx2} is identified as the safe stability region, as shown in Fig. 4 (i.e., the region highlighted in green). However, using the Bode plot to determine the stable region is slightly rough and insufficient, since a group of open-loop frequency responses should be obtained. It is, therefore, natural to quantify the relationship of f_{cx1} and f_{cx2} with *LCL* parameters, so that the design procedure can be simplified and synthesized. The open-loop transfer function in (5) can also be expressed in the *s*-domain as

$$G_{open}(s) = G_{pr}(s) \cdot G_{de}(s) \cdot V_{dc} \cdot G_{i2}(s) \tag{6}$$

Because the magnitude of the PR controller is near K_p around the resonant frequency [3] and $|G_{de}(s)|$ is always unity, (6) can be simplified as

$$G_{open}(s) = G_{i2}(s) \cdot K_p \tag{7}$$

Substituting (1) and (2) into (7) and then applying $s = j\omega$, the magnitude of the open-loop system $G_{open}(s)$ can be expressed as

$$\left|G_{open}(j\omega)\right| = \left|\frac{K_p n_1 \omega \cdot j + K_p}{-d_3\omega^3 \cdot j - d_2\omega^2 + d_1\omega \cdot j + d_0}\right| \tag{8}$$

When solving $|G_{open}(j\omega)| = 1$, it gives

$$\sqrt{K_p^2 n_1^2 \omega^2 + K_p^2} = \sqrt{\left(-d_3\omega^3 + d_1\omega\right)^2 + \left(-d_2\omega^2 + d_0\right)^2} \tag{9}$$

Eq. (9) can be used to calculate the crossover frequencies of the open-loop system $G_{open}(s)$. Unfortunately, it is very complicated and difficult to find a general roots-expression for (9). Here, the MATLAB "roots" function is adopted, which gives three roots of (9), and those are the crossover frequencies for $G_{open}(s)$, denoted as ω_{c1}, ω_{c2}, and ω_{c3}. Assuming that the ESRs r_1, r_2, and r_d change from 0 Ω to 1 Ω with a step of 0.01 Ω, the trajectories of f_{c1}, f_{c2} and f_{c3} (i.e., ω_{c1}, ω_{c2}, and ω_{c3} in Hz) are then given in Fig. 5. As it can be observed in Fig. 5, due to the ESRs, f_{c1} and f_{c3} are reduced, while f_{c2} becomes larger. However, the movement of the crossover frequencies is relatively small (all are less than 30 Hz), when the ESRs increase from 0 Ω to 1 Ω. Hence, neglecting the ESRs in the analysis may not affect f_{c1}, f_{c2}, and f_{c3} significantly. Furthermore, in practice, the ESRs of the inductor and capacitor are relatively small, when compared with the maximum of 1 Ω used in Fig. 5. Thus, the ESRs of the *LCL* filter are ignored to simplify the analysis. By doing so, n_1, d_2, and d_0 become zero and then (8) is reduced to

$$\left|G_{open}(j\omega)\right| = \left|\frac{K_p}{\left(-d_3\omega^3 + d_1\omega\right) \cdot j}\right| \tag{10}$$

Substituting (1) into (10), the crossover frequency of the open-loop system $G_{open}(s)$ can then be found by solving $|G_{open}(j\omega)| = 1$. Further simplification can be performed, leading to

$$\omega^3 + p\omega + q = 0 \quad \text{with} \quad p = -\omega_{res}^2, \quad q = \frac{K_p}{L_1\left(L_2 + L_g\right)C_f} \tag{11}$$

which is a one-variable cubic equation. Clearly, (11) has three roots related to the crossover frequencies f_{c1}, f_{c2}, and f_{c3} of the open-loop system $G_{open}(s)$. According to the Cardano's

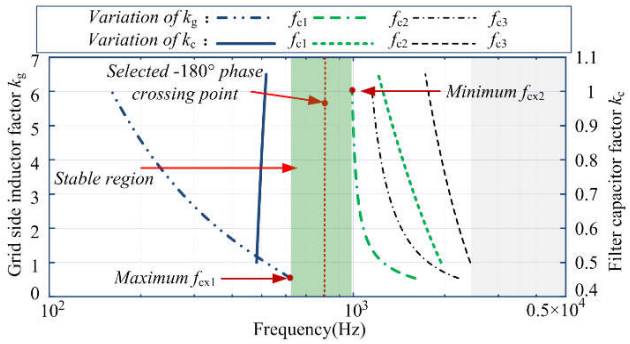

Fig. 6. Variation of crossover frequencies f_{c1}, f_{c2} and f_{c3} with different *LCL* filter parameters and grid impedance L_g.

method, all roots of the cubic equation (11) are real and unique, only if the following inequality is satisfied [30]:

$$\Delta = (\frac{q}{2})^2 + (\frac{p}{3})^3 = (\frac{K_p}{2L_1L_2C_f})^2 - (\frac{\omega_{res}^2}{3})^3 < 0 \tag{12}$$

If K_p is too large and (12) cannot be satisfied, the Cardano's method states that (11) has one real root and two complex roots, resulting in that the open-loop gain curve has only one crossover frequency. The only real root can be referred to as f_{c3} when the open-loop gain curve in Fig. 3 is moved upward to a large extent until f_{c1} and f_{c2} disappear. Obviously, in this case, the open-loop gain curve is always above 0 dB in the range $f < f_{res} < f_{c3}$, and the Nyquist stability criterion is difficult to meet, since the step phase change at f_{res} will contribute to a –180º-phase-crossing with the open-loop gain above 0 dB. Hence, (12) is a mandatory condition to stabilize the current control loop. In this paper, the gain of the PR controller K_p is designed according to (4), and hence, (12) can be simplified as

$$\Delta = (\frac{q}{2})^2 + (\frac{p}{3})^3 = \frac{\omega_b^2}{4V_{dc}^2} - \frac{\omega_{res}^2}{27} < 0 \tag{13}$$

It should be noted that the desired bandwidth ω_b is always smaller than the resonant frequency of the *LCL*-filter. Thus, (13) is always satisfied if the controller is designed according to (4). Subsequently, the three real-roots can be obtained. The first one denoted as ω_{c1} is referred to as the bandwidth of the control loop and can be calculated by using an equivalent *L* filter. According to (11), the three real-roots can be expressed as

$$\begin{cases} \omega_{c1} = 2\pi f_{c1} = R + T \\ \omega_{c2} = 2\pi f_{c2} = \lambda \cdot R + \lambda^2 \cdot T \\ \omega_{c3} = 2\pi f_{c3} = \left| \lambda^2 \cdot R + \lambda \cdot T \right| \end{cases} \tag{14}$$

where *R, T,* and λ are given as [30]

$$\begin{cases} R = \sqrt[3]{-\frac{K_p}{2L_1L_gC_f} + \sqrt{\left[\frac{K_p}{2L_1L_gC_f}\right]^2 + (\frac{\omega_{res}^2}{3})^3}} \\ T = \sqrt[3]{-\frac{K_p}{2L_1L_gC_f} - \sqrt{\left[\frac{K_p}{2L_1L_gC_f}\right]^2 + (\frac{\omega_{res}^2}{3})^3}} \end{cases} \tag{15}$$

$$\lambda = -1 + \sqrt{3}i \tag{16}$$

To explore how f_{c1} and f_{c2} vary with the grid impedance and *LCL*-filter parameters, the following is defined:

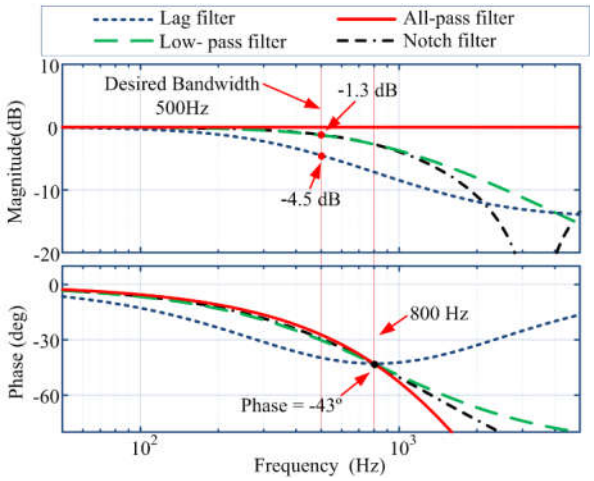

Fig. 7. Magnitude and phase responses of different digital filters.

TABLE II.
COMPARISON OF THE DIGITAL FILTERS.

Filter	Low pass filter	Phase-lag filter	Notch filter	All-pass filter
Gain Loss	**Small**	**Large**	**Small**	**Zero**
PM Loss	**Small**	**Large**	**Small**	**Small**

$$L_g = k_g L_2, \quad C_f = k_c C \tag{17}$$

where k_g is the grid impedance factor, k_c is the capacitance factor and *C* is the rated capacitance of the *LCL*-filter. Hence, k_g represents the possible variation of the grid impedance, and k_c is related to the capacitance change. Substituting the *LCL*-filter parameters from Table I, f_{c1}, f_{c2}, and f_{c3} in (14) are obtained, as shown in Fig. 6. As it can be observed in Fig. 6, when the capacitor factor k_c decreases to 0.5 from its nominal value 1 (i.e., corresponding to the 50%-degradation of capacitance), f_{c2} increases accordingly, but f_{c1} remains almost unchanged. On the other hand, when the grid impedance factor k_g increases from 0.5 to 6 (i.e., corresponding to the 50%-degradation of L_2 and the variation of the grid impedance from 0 to 10 mH), both f_{c1} and f_{c2} decrease from its normal value (when k_g = 1). Fig. 6 also indicates that in the pre-defined variation ranges of L_{grid} and *LCL* filter parameters, f_{c2} is always larger than f_{c1}. This means that there is a frequency range that the open-loop gain can be maintained below 0 dB, as shown in the green area in Fig. 6. This highlighted area is related to the stable region shown in Fig. 4, where the open-loop Bode plot was adopted. Once the −180°-phase crossing of the open-loop system is placed in this region (i.e., the green area in Fig. 6), the *LCL*-filtered converter has high robustness against large variations of the grid impedance and *LCL*-filter parameters. The optimal −180°-phase-crossing point can be selected at the mean value of the maximum frequency f_{cx1} and the minimum frequency f_{cx2}, implying the same tolerant range for both f_{c1} and f_{c2} variations.

C. *Digital Filters for Phase Reshaping*

Based on the above discussions, there is thus a need to reshape the open-loop phase to ensure the GCF control stability. In this case, the additional lagging phase should be implemented, as it was also discussed in [19]. In this section, vari-

ous digital filters are then employed to realize the phase reshaping (i.e., additional lagging phase), so that the current controller design can be independent of the active damping design. Nevertheless, a digital filter should be selected with the following requirements:

1) The filter should be able to provide a lagging phase in the stable region or at the selected −180°-phase-crossing point f_{dp}.
2) The digital filter gain should be as high as possible in the frequency range below f_{dp} to maintain the bandwidth.

With the above concerns, [22] has given a comprehensive comparison between the low-pass filter (LPF), a phase-lag filter (LF) [12], a notch filter (NF) [19], and an AF [32] with lagging phase characteristics. As it has been benchmarked, all the filters provide the same lagging phase at a specific frequency (e.g., −45º at 800 Hz). According to the transfer functions given in [22], the frequency responses of the selected digital filters are plotted in Fig. 7. As can be seen in Fig. 7, using an LF for the phase reshaping will sacrifice the control bandwidth and its large lagging phase will reduce the phase margin (PM). In contrast, the LPF, the NF, and the AF have almost the same phase response in the low-frequency range, while the AF is the best in terms of magnitude response. The features of the selected filters are also summarized in Table II. This further confirms that the AF is the best candidate for the phase reshaping in terms of control bandwidth degradation and PM loss among the selected.

III. PROPOSED PHASE RESHAPING WITH AN ALL-PASS FILTER

Section III demonstrates that the AF is the promising candidate to reshape the open-loop phase. This concept was firstly adopted in [21] to guarantee zero phase at the resonant frequency. In this section, a novel design method is proposed for the AF-based active damping. An AF is employed to reshape the phase crossing of the open-loop system at a desired point that is in the stable region identified in Section II in a way that the active damping is robust against grid impedance and *LCL*-filter parameter variations.

A. All-pass filter design

The AF has a 0-dB gain in the entire frequency range, and its simplest form can be expressed as [32]

$$G_{AF}(z)=\frac{-rz+1}{z-r},\quad 0<r<1 \tag{18}$$

with r being the pole of the AF. The phase response of the AF with different poles r is given in Fig. 8, where it is demonstrated that the increase of the pole r results in larger lagging phase. Hence, it is possible to adjust the pole r to achieve the desired phase lag at a specific frequency. The phase of the AF can be derived from (18) as

$$\theta_{AF}(\omega)=-\omega T_s+2\arctan\frac{r\sin\omega T_s}{1-r\cos\omega T_s} \tag{19}$$

If a phase lag $\theta_{\omega dp}$ is specified at the desired frequency ω_{dp}, the pole r can thus be solved as

$$r=\frac{\tan\left[0.5\left(\theta_{\omega dp}+\omega_{dp}T\right)\right]}{\tan\left[0.5\left(\theta_{\omega dp}+\omega_{dp}T\right)\right]\cos\omega_{dp}T-\sin\omega_{dp}T} \tag{20}$$

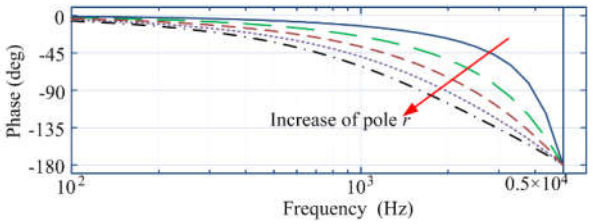

Fig. 8. Phase of the all-pass filter with different poles r.

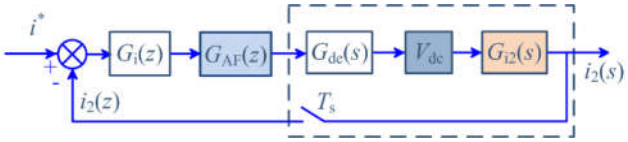

Fig. 9. Current control loop when the all-pass filter is introduced to reshape the phase.

It is worth mentioning that the first-order AF can provide the maximum phase of −180º. Thus, one first-order AF is able to provide sufficient phase to stabilize the GCF-controlled *LCL*-filtered converter, as it will be explained in the following.

B. Proposed design method for the AF-based active damping

Fig. 9 shows the current control loop with an AF in the forward path for the phase reshaping. Accordingly, the open-loop transfer function of the current control can be expressed in the z-domain as

$$G_{open}(z)=G_{pr}(z)\cdot G_{AF}(z)\cdot Z\left\{G_{de}(s)\cdot V_{dc}\cdot G_{i1}(s)\right\} \tag{21}$$

It is assumed that the PR controller does not contribute so much phase at the first crossover frequency f_{c1} [3], i.e., $\angle G_{pr}(e^{j2\pi f_{c1}T_s})\approx 0$. Then, by approximating the phase behavior of the *LCL* filter as a single *L* filter [3], [22], the phase of the open-loop system can be derived as

$$\begin{aligned}\theta_{open}(f)&=\angle G_{i2}\left(e^{j2\pi fT_s}\right)+e^{-j2\pi fT_s}+\angle G_{AF}\left(e^{j2\pi fT_s}\right)\\&=\begin{cases}-\dfrac{\pi}{2}-3\pi\dfrac{f}{f_s}+\theta_{AF}(f), & f<f_{res}\\ -\dfrac{3\pi}{2}-3\pi\dfrac{f}{f_s}+\theta_{AF}(f), & f>f_{res}\end{cases}\end{aligned} \tag{22}$$

The phase reshaping aims to place the −180°-phase-crossing point f_{dp} between the first and the second crossover frequencies f_{c1} and f_{c2}, i.e., $f_{c1}<f_{dp}<f_{c2}<f_{res}$. Hence, only the phase with $f<f_{res}$ in (22) is considered in the analysis. From (22), the desired phase of the AF at f_{dp} can be expressed as

$$\theta_{AF}(f_{dp})=\angle G_{AF}(f_{dp})=-\frac{\pi}{2}+3\pi\frac{f_{dp}}{f_s} \tag{23}$$

which shows that the largest required lagging phase is -0.5π when $f_{dp}=0$. It means that only one first-order AF is enough for the phase reshaping, as mentioned previously. Referring to Section II, the recommended −180°-phase-crossing point f_{dp} is the mean value of f_{cx1} and f_{cx2} in Fig. 6. If a 50%-reduction of the *LCL*-filter parameters and a variation of the grid impedance from 0 to 10 mH are considered, f_{dp} can be calculated as 815 Hz. Substituting f_{dp} into (23), the phase that the AF should provide is −45º ($\theta_{AF}=-45º$). Finally, the pole of the AF can be calculated according to (20), which gives $r=0.222$.

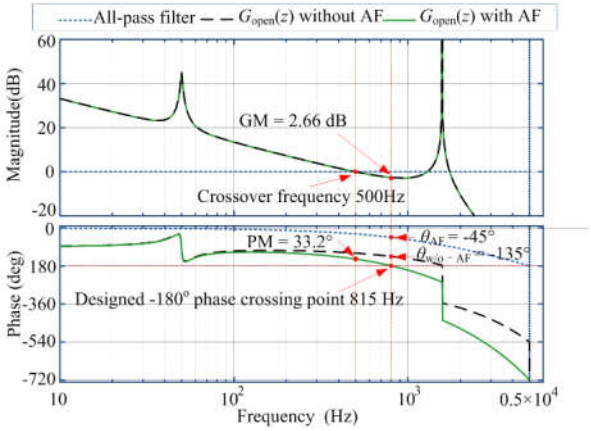

Fig. 10. Bode plot of the open-loop system with an all-pass filter.

Subsequently, the Bode plot of the open-loop system, i.e., (21), can be obtained as shown in Fig. 10 with r = 0.222 and the parameters are given in Table I. As it can be seen in Fig. 10, the −180°-phase-crossing of the open-loop system $G_{open}(z)$ with the AF occurs at the designed frequency of f_{dp} = 815 Hz, where the gain margin (GM) is 2.66 dB and the PM at f_{c1} is reduced from 60° to 33.2°. This PM reduction is the major drawback of all the filter-based active damping methods. In other words, a trade-off between the PM decease and the damping effectiveness should be made. In addition, there is no −180°-phase-crossing with the gains above 0 dB in Fig. 10. Consequently, the current control system stability is guaranteed. Fig. 11 further shows the root loci in the z-plane of the overall current control system when the grid impedance and the *LCL*-filter parameters vary. Observations in Fig. 11(a) indicate that the control system maintains the stability when the filter capacitance decreases to 50% of the rated. This is in agreement with the discussions in Section II—the control loop keeps stable with a 50%-degradation in the filter capacitance. However, when the filter capacitance further increases to 120% or decreases to 25% of the rated, the closed-loop poles (red in Fig. 11a) will move outside the unit circle, indicating that the current control system becomes unstable even with the AF. On the other hand, Fig. 11(b) shows that although the grid impedance L_{grid} varies between 0 mH (a very strong grid) and 10 mH (a very weak grid), the system is always stable. Thus, the proposed AF-based active damping can keep the current control loop stable in the pre-defined range. That is, it can tolerate a wide range of grid impedance variations and *LCL*-filter parameter drifts, being highly robust.

C. Design guideline for the proposed active damping

To summarize the above discussion, the flowchart of the proposed algorithm is shown in Fig. 12. At ***Step*** 1 and ***Step*** 2, the *LCL*-filter parameter and the PR controller are designed referring to [33], [34] and Eq. (4), respectively. Then, at ***Step*** 3, if the *LCL*-filter resonant frequency f_{res} is larger than the critical frequency f_{cri} ($f_{cri} = f_s/6$, and $f_{cri} < f_{res}$), the current control loop is inherently stable without active damping and the current control design can be performed. Otherwise, an AF is adopted to stabilize the current control loop, as discussed above. A variation range of the grid impedance and *LCL*-filter parameters can be assumed to define the robustness level of the proposed active damping. Eqs. (14) - (17) are then em-

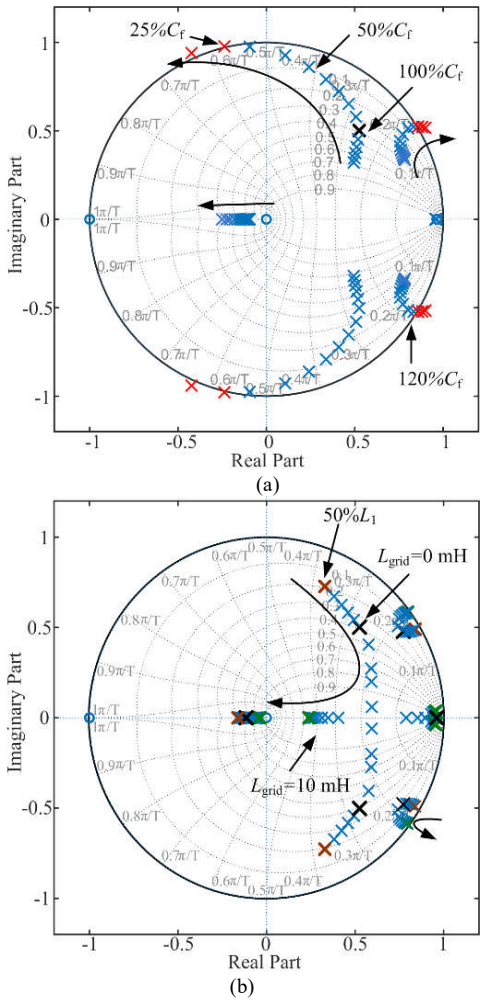

Fig. 11. Pole and zero location of the overall system when the grid impedance and the *LCL*-filter parameters are changed: (a) filter capacitor C_f changes and (b) grid impedance L_{grid} varies (0 mH to 10 mH).

ployed to calculate the variation range of the crossover frequency and find the desired −180°-phase-crossing point f_{dp}, as mentioned in Section II.B. After that, the lagging phase θ_{AF} that the AF should provide at the selected frequency crossing point f_{dp} can be calculated according to (23), as ***Step*** 4. Finally, according to (20), the pole r of the AF is calculated at ***Step*** 5. It is worth pointing out that *the implementation of the control bandwidth design in* ***Step 2*** will not change with the following steps. That is, the PR controller design is independent of the active damping design, which is also one of the objectives of the proposed method—to separate the design of the current controllers and active damping. Once the active damping design is finalized, it can be easily applied to other PWM converters.

IV. AF Application in The CCF Control

It has been pointed in [21] and also this paper that using an AF is an easy way to stabilize the GCF control. However, the CCF control is practically preferred in industrial applications, as the current sensors are typically installed in the converter. Thus, it is necessary to discuss the possibility of applying the AF active damping to the CCF control. Fig. 13 shows the inner current loop of the *LCL*-filtered converter with the CCF

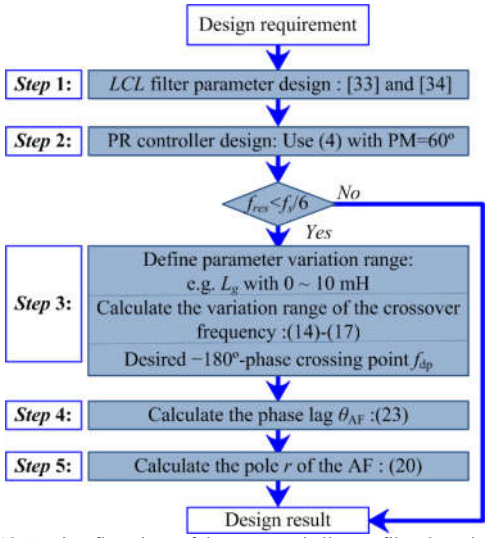

Fig. 12. Design flowchart of the proposed all-pass filter-based active damping.

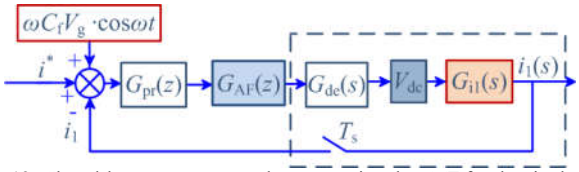

Fig. 13. Closed-loop current control system using the CCF for the single-phase AC/DC converter with an *LCL* filter.

control and AF for active damping, where $G_{i1}(s)$ is the transfer function of the *LCL*-filter from the converter output voltage v_{con} to the converter side current i_1 as

$$G_{i1}(s)=\frac{i_1(s)}{v_{con}(s)}=\frac{L_gC_fs^2+1}{s\cdot\left[L_1L_gC_f\cdot s^2+L_1+L_g\right]} \tag{24}$$

which has an anti-resonant frequency at $f_{at\_res}=1/L_gC_f$ with a 180°-phase change. As shown in Fig. 13, an additional term $\omega C_fV_g\cdot\cos\omega t$ is added in the current reference i^* to compensate the reactive power exchange from the filter capacitor. Subsequently, the open-loop transfer function of the CCF control with an AF is given as

$$G_{open}(z)=G_{pi}(z)\cdot G_{AF}(z)\cdot Z\left\{G_{de}(s)\cdot V_{dc}\cdot G_{i1}(s)\right\} \tag{25}$$

According to [19], the unstable region of the GCF and CCF control can be partitioned into three sub-regions, namely GCF I (0~ $f_s/6$), CCF II ($f_s/6$~ $f_s/3$), and CCF III ($f_s/3$~ $f_s/2$), as shown in Fig. 14. It was also revealed in [19] that introducing proper lagging phase helps to make the −180°-phase-crossing happen before the resonant frequency, and thus it can maintain the stability of the current control loop in GCF I and CCF III. On the contrary, as mentioned in [19] that the leading phase is preferred in CCF II, the AF with lagging phase is not suitable for the current control in the region of the CCF II. Thus, this paper will not discuss using an AF to stabilize the current control in the CCF II region.

For the CCF III, the active damping design is directed to the method in [19] with dual notch filters. In [19], the notch frequency is designed at the Nyquist frequency, and the notch filters only provide lagging phase with the maximum being −180°. Then, the phase of the open-loop system is pulled

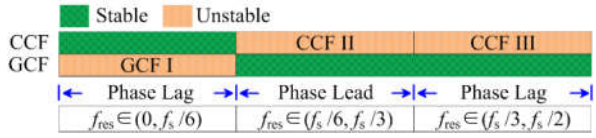

Fig. 14. Stability regions of the *LCL*-filtered PWM converter considering a time delay of $1.5T_s$, when either the grid-side current (GCF) or the converter-side current (CCF) is fed back to the control loop [19].

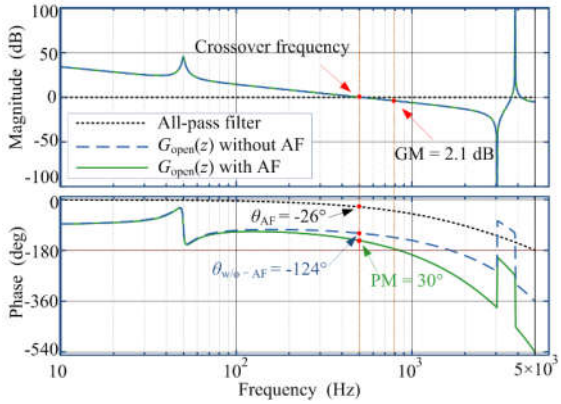

Fig. 15. Bode plot of the open-loop system with the CCF control with an all-pass filter (region CCF III: CCF control with f_{res} in $\{f_s/3, f_s/2\}$).

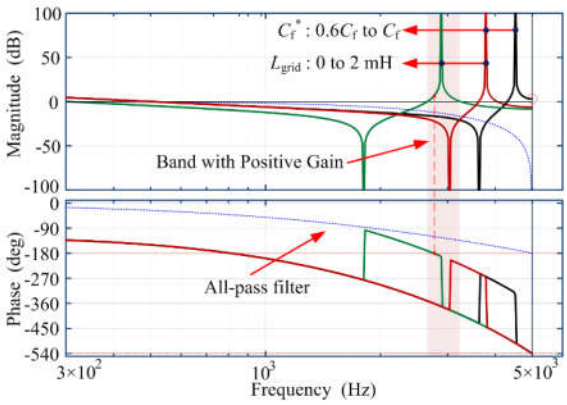

Fig. 16. Bode plot of the all-pass filter based active damping in the region of CCF III with different f_{res}. (CCF control with f_{res} located in $\{f_s/3, f_s/2\}$).

down to avoid the −180°-phase-crossing around the resonant frequency f_{res}. The NF is also required to ensure a sufficient PM at the crossover frequency f_{c1} (e.g., PM = 30°). This design is then applied to the AF-based active damping, since an AF also can provide maximum −180°-phase before the Nyquist frequency. Moreover, it is possible to manage the PM at f_{c1}. Considering a capacitor of 2.5 μF for the *LCL*-filter (the other parameters remain), the resonant frequency will be moved to the region of CCF III ($f_s/3 < f_{res}$ = 3852 Hz $< f_s/2$). In this case, the open-loop Bode plot with an AF is given in Fig. 15, where the AF is designed to provide the phase of −26° to guarantee the PM at f_{c1} (PM = 30°). As observed in Fig. 15, the lagging phase from the AF successfully pulls down the open-loop phase, and consequently, no −180°-phase crossing occurs with the gain above 0 dB. Thus, the system is stable, and the AF is able to stabilize the CCF control system.

Furthermore, the Bode plots of $G_{open}(z)$ with various grid impedance L_{grid} and filter capacitors C_f are given in Fig. 16. As shown in Fig. 16, $G_{open}(z)$ has two large phase changes (180°-change). These are induced by the resonant frequency f_{res} and

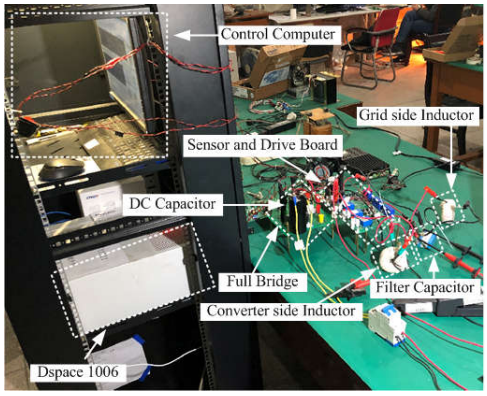

Fig. 17. Laboratory experimental prototype of a single-phase *LCL*-filtered converter.

the anti-resonant frequency f_{at_res}. The system $G_{open}(z)$ is originally stable if there are no such parameter variations. However, when L_{grid} increases to 2 mH, the stability is lost due to that another −180º-phase-crossing emerges in the frequency band with positive gains around the resonant frequency (see Fig. 16, the shaded area). Moreover, in the case of a 40%-decrease in the filter capacitor, the third crossover frequency f_{c3} is missing (beyond the Nyquist frequency), as shown in Fig. 16, and $G_{open}(z)$ becomes unstable. This is because $G_{open}(z)$ has a positive gain with the phase being −540º at the Nyquist frequency. Considering the folding effect of digital control systems, this phenomenon is equivalent to a −180º-phase-crossing with a positive gain [33], and the system becomes unstable. In all, compared with the GCF control, applying an AF to the CCF control gives limited tolerance of the grid impedance L_{grid} and filter parameter variations.

V. Experimental Results and Discussion

To verify the proposed AF-based active damping, a single-phase *LCL*-filtered converter prototype has been built, as shown in Fig. 17. The converter parameters are given in Table I. The DC capacitor is designed to limit the DC voltage ripple within 10% of its average value, and a 2200μF capacitance is selected in the experimental setup. The converter-side inductor L_1 is designed according to the peak-to-peak current ripple ΔI_{Lx} being 30% of the rated current [33], resulting in L_1 = 1.5 mH, which is chosen as 1.8 mH due to the lab availability. The grid-side inductor L_2 is selected as 1.1 mH, with which the peak-to-peak current ripple will be further reduced to be below 1% of the rated current [34]. The control systems were implemented in a dSPACE DS 1006 system. The inner current control algorithm is developed according to the control schemes shown in Figs. 9 and 13, for the GCF and CCF control, respectively. To place the resonant frequency in different unstable regions, the filter capacitance is selected as 15 μF (GCF) and 2.5 μF (CCF). Experiments have been performed on the system firstly with the GCF control and the AF. Due to the filter capacitance of 15 μF, the resonant frequency calculated as f_{res} = 1527 Hz, where thus damping is required. According to the design procedure in Section IV, the AF should reshape the −180º-phase-crossing of the open-loop

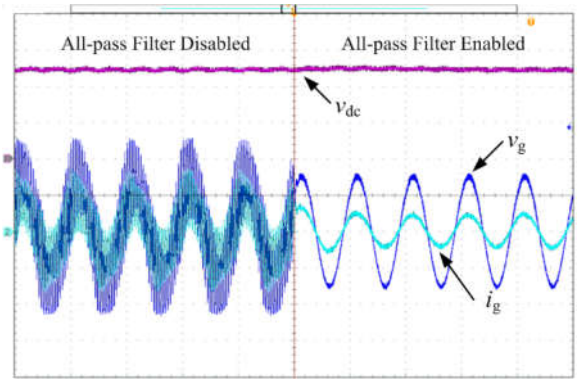

Fig. 18. Performance of the all-pass filter-based active damping in the region of GCF I: grid current i_g: 10 A/div, grid voltage v_g: 100 V/div, DC output voltage v_{dc}: 100 V/div, and time: 20 ms/div.

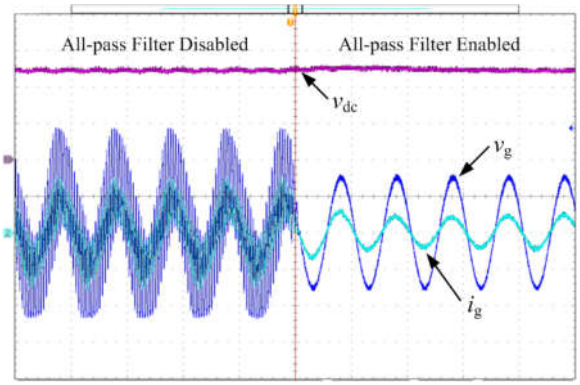

Fig. 19. Performance of the all-pass filter-based active damping in the region of GCF I with 2-mH additional grid impedance: grid current i_g: 10 A/div, grid voltage v_g: 100 V/div, DC output voltage v_{dc}: 100 V/div, and time: 20 ms/div.

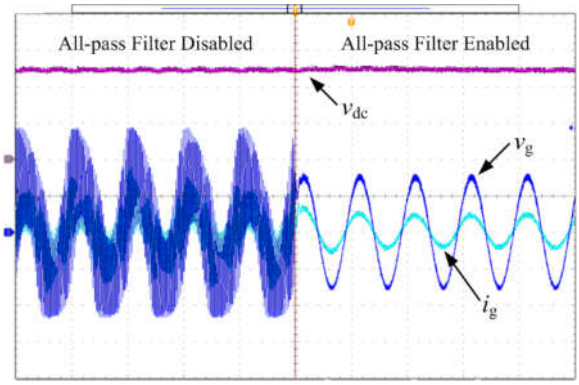

Fig. 20. Performance of the all-pass filter-based active damping in the region of GCF I with a 50%-degradation of the filter capacitance C_f: grid current i_g: 10 A/div, grid voltage v_g: 100 V/div, DC output voltage v_{dc}: 100 V/div, and time: 20 ms/div.

system at 815 Hz, which allows the grid impedance variation from 0 to 10 mH and up to 50% degradation in the filter capacitance. Furthermore, according to Fig.2, due to use of the notch filter to minimize the impact of DC ripple voltage on the current reference, the control bandwidth of the voltage control loop is below 20Hz, which is much lower than the current loop.

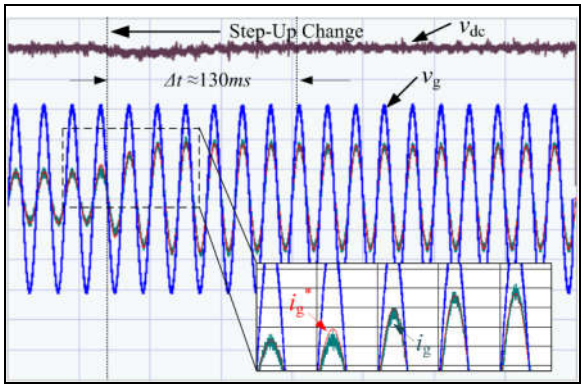

Fig. 21. Dynamic performance of the all-pass filter-based active damping in the region of GCF I with a step-up load change (4 A to 9 A): grid current i_g: 5 A/div, grid voltage v_g: 50 V/div, DC output voltage v_{dc}: 50 V/div, and time: 50 ms/div.

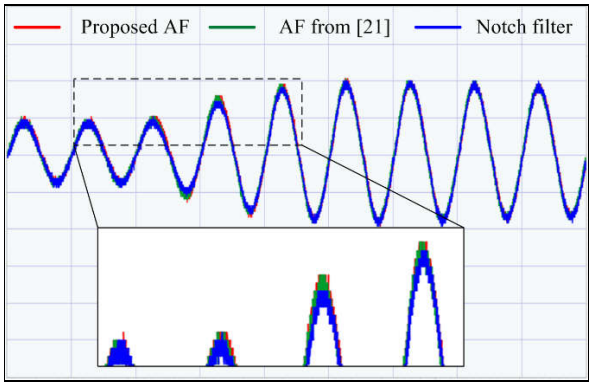

Fig. 22. Performance comparison (grid current) of the *LCL*-filtered converter with various active damping methods: grid current i_g: 5 A/div and time: 20 ms/div.

Fig. 18 shows the experimental results, which indicate that the resonance occurs without the AF. In the next case, an external inductor L_{grid} is added as the grid impedance to emulate a weak grid system. The results given in Fig. 19 demonstrate that the system can be stabilized with the designed AF. When disabling the AF, the converter input current i_g contains large oscillations, i.e., being unstable. This can further be seen in Fig. 20, where the filter capacitance is assumed to have a 50%-degradation. In all, Figs. 18-20 have verified the effectiveness of the AF-based active damping for the *LCL*-filtered converters with the GCF control. More importantly, the proposed solution is robust against grid impedance variations and *LCL*-filter parameter drifts. In addition, the dynamic performance of the proposed active damping method is explored, where a step change of the reference grid current from 4 A to 9 A (440 W to 990 W) is performed. Results are shown in Fig. 21, which demonstrates that the measured grid current follows its reference i_g^* with fast dynamics and negligible transient oscillations. The DC voltage dip during the transient interval has also been kept within 9 V and recovered back to the 225-V DC voltage reference within 130 ms.

Fig. 22 shows the transient responses of the LCL-filtered converter with various digital-filter-based active damping methods. To make a fair comparison, the AF designed from [21] and NF from [19] are compared with the proposed method, since they are the filter-based method and no additional sensor required. The comparison results shown in Fig. 22 suggest that the proposed AF and the AF from [21] have different phase lag at the crossover frequency f_{c1}, but they have almost the same tracking performance. Thus, the AF lagging phase will not affect the dynamics, as the control bandwidth is kept unchanged. Moreover, the NF-based method is slightly slower than the AF-based method. This is because the NF has negative gains below the Nyquist frequency, resulting in the reduced crossover frequency f_{c1} as well as lowered control bandwidth.

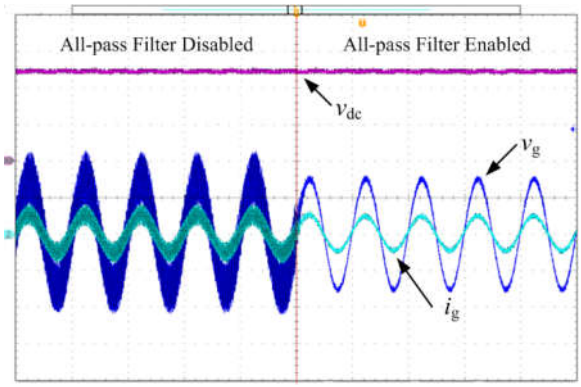

Fig. 23. Performance of the all-pass filter-based active damping in the region of CCF III: grid current i_g: 10 A/div, grid voltage v_g: 100 V/div, , DC output voltage v_{dc}: 100 V/div, and time: 20 ms/div.

Following, the CCF control for the single-phase AC/DC converter system is tested according to Fig. 13. In this case, the filter capacitance is 2.5 μF and the resonant frequency of the *LCL* filter is f_{res} = 3852 Hz, which is in the region of CCF III. The AF is designed according to Section V that ensures a PM of 30º at the crossover frequency f_{c1}. As a result, the AF should provide a phase of −26º at the desired frequency f_{c1} = 500 Hz, and the pole of the AF is then obtained as r = 0.1957. Fig. 23 shows the performance of the converter system with the AF. As it can be observed in Fig. 23, the AF is able to stabilize the CCF control in the region of CCF III. As anticipated, the resonance appears when the AF is disabled. Compared with the GCF, the grid voltage v_g and current i_g have slight phase difference, because the reactive power compensation term $\omega C_f V_g \cdot \cos\omega t$ cannot perfectly match the real power consumed by the capacitor. Nevertheless, the above experimental results have confirmed the effectiveness of the AF-based active damping by properly rephrasing the phase of the open-loop system.

VI. CONCLUSIONS

In this paper, a novel AF-based active damping method is proposed for the grid-current feedback-controlled converter with an *LCL*-filter. Based on the stability analysis with different resonant frequencies, a stable region of −180º-phase crossing is identified considering a predefined range of grid impedance changes and *LCL*-filter parameter variations. Once the phase of the current control loop is reshaped to the identified stable region, the system stability can be ensured. Various digital filter-based active damping methods are benchmarked, which has demonstrated that the AF features a unity gain and adjustable lagging phase in the entire frequency range, being a promising solution for phase reshaping. Using an AF enables the independent design of the current controller and the AF-

based active damping. Furthermore, applying the AF to the converter-side current control is also discussed, which has confirmed that the AF is not very suitable for the region of the CCF II, since using an AF to provide leading phase may bring another −180º-phase crossing point at high frequencies. In the region of CCF III, the AF can stabilize the entire system, but with limited tolerance of the grid impedance and parameter variations. Experimental tests are provided, which have verified that the proposed AF-based active damping method can ensure system stability while maintaining fast dynamics.

REFERENCES

[1] E. Twinning and D. G. Holmes, "Grid current regulation of a three-phase voltage source converter with an LCL input filter," *IEEE Trans. Power Electron*., vol. 18, no. 3, pp. 888–895, May 2003.

[2] M. Liserre, R. Teodorescu, and F. Blaabjerg, "Stability of photovoltaic and wind turbine grid-connected converters for a large set of grid impedance values," *IEEE Trans. Power Electron.,* vol. 21, no. 1, pp. 263– 272, Jan. 2006.

[3] S. Parker, B. P. McGrath, and D. G. Holmes, "Region of active damping control for LCL filters," *IEEE Trans. Ind. Appl.,* vol. 50, no. 1, pp. 424-432, Jan.-Feb. 2014.

[4] J.G. Wang, J. D. Yan, L. Jiang, and J.Y Zou, "Delay-Dependent Stability of Single-Loop Controlled Grid-Connected Converters with *LCL* Filters," *IEEE Trans. Power Electron.,* vol. 31, no. 1, pp. 734-757, Jan. 2016.

[5] C. Zou, B. Liu, S. Duan, and R. Li, "Influence of Delay on System Stability and Delay Optimization of Grid-Connected Converters with LCL Filter," *IEEE Trans. Ind. Inform*., vol. 10, no. 3, pp. 1775-1784, Aug. 2014.

[6] R. Beres, X. Wang, F. Blaabjerg, M. Liserre and C. Bak, "Optimal Design of High-Order Passive-Damped Filters for Grid-Connected Applications," *IEEE Trans. Power Electron.,* vol. 31, no. 3, pp. 2083-2098, 2016.

[7] W. Wu, Y. Li, Y. He, H. S. H. Chung, M. Liserre, and F. Blaabjerg, 'Damping Methods for Resonances Caused by LCL-filter-based Current-controlled Grid-tied Power Converters: An Overview,' *IEEE Trans. Ind. Electron*., vol. 64, no. 9, pp. 7402-7413, 2017.

[8] X. Wang, F. Blaabjerg, and P. C. Loh, "Virtual RC damping of *LCL*-filtered voltage source converters with extended selective harmonic compensation," *IEEE Trans. Power Electron.*, vol. 30, no. 9, pp. 4726-4737, Sep. 2010.

[9] D. Pan, X. Ruan, C. Bao, W. Li, and X. Wang, "Capacitor-current feedback active damping with reduced computation delay for improving robustness of LCL-type grid-connected converter," *IEEE Trans. Power Electron*., vol. 29, no. 7, pp. 3414-3427, Jul. 2014.

[10] X. Li, J. Fang, Y. Tang, X. Wu, and Y. Geng, "Capacitor-voltage feedforward with full delay compensation to improve weak grids adaptability of LCL-filtered grid-connected converters for distributed generation systems," *IEEE Trans. Power Electron*., vol. 33, no. 1, pp. 749-764, Jan. 2018.

[11] Z. Xin, P. C. Loh, X. Wang, F. Blaabjerg, and Y. Tang, "Highly accurate derivatives for LCL-filtered grid converter with capacitor voltage active damping," *IEEE Trans. Power Electron*., vol. 31, no. 5, pp. 3612-3625, May 2016.

[12] R. Pena-Alzola, M. Liserre, F. Blaabjerg, R. Sebastian, J. Dannehl, and F. W. Fuchs, "Systematic Design of the Lead-Lag Network Method for Active Damping in LCL-Filter Based Three Phase Converters," *IEEE Trans. Ind. Informat*., vol. 10, no.1, pp. 43- 52, Feb. 2014.

[13] H. Komurcugil, N. Altin, S. Ozdemir, and I. Sefa, "Lyapunov-function and proportional-resonant-based control strategy for single-phase gridconnected VSI with LCL filter," *IEEE Trans. Ind. Electron.*, vol. 63, no. 5, pp. 2838-2849, May 2016.

[14] T. Roinila, M. Vilkko, and J. Sun, "Online grid impedance measurement using discrete-interval binary sequence injection," *IEEE J. Emerg. Sel. Top. Power Electron.*, vol. 2, no. 4, pp. 985-993, Dec. 2014.

[15] S. Cobreces, E. J. Bueno, D. Pizarro, F. J. Rodriguez, and F. Huerta, "Grid Impedance monitoring system for distributed power generation electronic interfaces," *IEEE Trans. Instrum. Meas.*, vol. 58, no. 9, pp. 3112-3121, Sep. 2009.

[16] M. Liserre, F. Blaabjerg, and R. Teodorescu, "Grid impedance estimation via excitation of LCL-filter resonance," *IEEE Trans. Ind. Appl.*, vol. 43, no. 5, pp. 1401-1407, Sep./Oct. 2007

[17] T. Roinila, J. Huusari, and M. Vilkko, "On frequency-response measurements of power-electronic systems applying MIMO identification techniques,'' *IEEE Trans. Ind. Electron*., vol. 60, no. 11, pp. 5270-5276, Nov. 2013.

[18] M. Liserre, A. Dell'Aquilla, and F. Blaabjerg, "Genetic algorithm based design of the active damping for a LCL-filter three-phase active rectifier," *IEEE Trans. Power Electron*., vol. 19, no. 1, pp. 234-240, Jan. 2003.

[19] W. Yao, Y. Yang, X. Zhang, F. Blaabjerg, and P. C. Loh, "Design and analysis of robust active damping for LCL filters using digital notch filters," *IEEE Trans. Power Electron.*, vol. 32, no. 3, pp. 2360-2375, Mar. 2017.

[20] R. Peña Alzola, M. Liserre, F. Blaabjerg, M. Ordonez, and T. Kerekes, "A self-commissioning notch filter for active damping in a three-phase LCL-filter-based grid-tie converter," *IEEE Trans. Power Electron*., vol. 29, no. 12, pp. 6754-6761, Dec. 2014.

[21] J. R. Pérez, E. J. Bueno, R. Peña-Alzola, and A. R. Cabero, "All-Pass-Filter-based Active Damping for VSCs with LCL Filters Connected to Weak Grids," *IEEE Trans. Power Electron.*, vol. 33, no. 11, pp. 9890-9901, Jan. 2018.

[22] W. Yao, Y. Yang, Y. Xu, F. Blaabjerg, S. Liu, and G. Wilson, "Active damping of LCL filters with All-pass filters considering grid impedance variations and parameter drifts," in *Proc. IEEE Energy Convers. Congr. Expo*., 2018, pp. 4915–4921.

[23] R. Pena-Alzola, J. R. Perez, E. Bueno, F. Huerta, D. C. Gaona, M. Liserre and G. M. Burt, "Robust Active Damping in *LCL*-filter based Medium-Voltage Parallel Grid-Converters for Wind Turbines," *IEEE Trans. Power Electron*., vol. 33, no. 12, pp. 10846-10857, Feb. 2018.

[24] X. Wang, X. F. Blaabjerg, and P. C. Loh, "Grid-current-feedback active damping for *LCL* resonance in grid-connected voltage source converters," *IEEE Trans. Power Electron.*, vol. 3, no. 1, pp. 213-223, Jan. 2016.

[25] V. Miskovic, V. Blasko, T. M. Jahns, A. H. C. Smith, and C. Romenesko, "Observer based active damping LCL resonance in grid-connected voltage source converters," *IEEE Trans. Ind. Appl*., vol. 50, no. 6, pp. 3977-3985, Nov./Dec. 2010.

[26] D. Yang, X. Ruan, and H. Wu, "Impedance shaping of the grid connected converter with LCL filter to improve its adaptability to the weak grid condition," *IEEE Trans. Power Electron*., vol. 29, no. 11, pp. 5795-5805, Nov. 2014.

[27] X. Wu, X. Li, X. Yuan, and Y. Geng, "Grid harmonics suppression scheme for LCL-type grid-connected converters based on output admittance revision," *IEEE Trans. Sustain. Energy*, vol. 6, no. 2, pp. 411-421, Apr. 2015.

[28] X. Fu and S. Li, "Control of single-phase grid-connected converters with LCL filters using recurrent neural network and conventional control methods," *IEEE Trans. Power Electron.*, vol. 31, no. 7, pp. 5354-5364, Jul. 2016.

[29] Y. Tang, Z. Qin, F. Blaabjerg, and P. C. Loh, "A dual voltage control strategy for single-phase PWM converters with power decoupling function," *IEEE Trans. Power Electron.*, vol. 30, no. 12, pp. 7060-7071, Dec. 2015.

[30] R. Wituła and D. Słota, "Cardano's formula, square roots, Chebyshev polynomials and radicals," *J. Math. Anal. Appl*., vol. 363, no. 2, pp. 639-647, 2010.

[31] A. G. Radwan, A. M. Soliman, and A. S. Elwakil, "First-order filters generalized to the fractional domain," *J. Circuits Syst. Comput*., vol. 17, pp. 55-66, Feb. 2008.

[32] S.C. Pei and C.C. Tseng, "IIR multiple notch filter based on All-pass filter," *IEEE Trans. Circuits Syst. II, Analog Digit. Signal Process*., vol. 44, no. 2, pp. 133-136, Feb. 1997.

[33] Y. Tang, W. Yao, P. C. Loh, and F. Blaabjerg, "Design of LCL-Filters with LCL Resonance Frequencies beyond the Nyquist Frequency for Grid-Connected Converters," *IEEE J. Emerg. Sel. Top. Power Electron.,* vol. 4, no. 1, pp. 3-14, July. 2015.

[34] A. Reznik, M. Simoes, A. Al-Durra, and S. Muyeen, "LCL filter design and performance analysis for grid-interconnected systems," *IEEE Trans. Ind. Appl.,* vol. 50, no. 2, pp. 1225-1232, Mar./Apr. 2014.

[35] S. R. Choudhury, A. Das, S. Anand, S. Tungare, and Y. Sonawane, "Adaptive shunt filtering control of UPQC for increased nonlinear loads," *IET Power Electron*., vol. 12, no. 2, pp. 330-336, 2019.R. Teodorescu, F. Blaabjerg, M. Liserre, and A. Dell'Aquila, "A stable three-phase *LCL*-filter based active rectifier without damping," in *Proc. of IEEE IAS Annu. Meeting*, pp. 1552-1557, 2003.

Wenli Yao (S'14–M'17) received the B.S., M.S., and Ph.D. degrees in electrical engineering from Northwestern Polytechnical University, Xi'an, China, in 2009, 2012, and 2017, respectively. From 2013 to 2015, he was a Visiting Scholar at Aalborg University, Aalborg, Denmark. From 2017 to 2019, he was a Research Fellow with the Rolls-Royce@NTU Corporate Lab, School of Electrical and Electronics Engineering, Nanayang Technological University, Singapore. Since May 2019, he has been with Northwestern Polytechnical University, Xi'an, China, as an Associate Professor. His research interests include current control, grid-connected inverter, multipulse converter, and power decoupling.

Yan Xu (S'10-M'13-SM'19) received the B.E. and M.E degrees from South China University of Technology, Guangzhou, China in 2008 and 2011, respectively, and the Ph.D. degree from The University of Newcastle, Australia, in 2013. He is now the Nanyang Assistant Professor at School of Electrical and Electronic Engineering, Nanyang Technological University, Singapore. Previously, he held The University of Sydney Postdoctoral Fellowship in Australia. His research interests include power system stability and control, microgrid, and data-analytics for smart grid applications. Dr Xu is an Editor for IEEE TRANSACTIONS ON SMART GRID, *CSEE Journal of Power and Energy Systems*, and an Associate Editor for *IET Generation, Transmission & Distribution*.

Yongheng Yang (SM'17) received the B.Eng. degree in electrical engineering and automation from Northwestern Polytechnical University, Shaanxi, China, in 2009 and the Ph.D. degree in electrical engineering from Aalborg University, Aalborg, Denmark, in 2014.

He was a postgraduate student at Southeast University, China, from 2009 to 2011. In 2013, he spent three months as a Visiting Scholar at Texas A&M University, USA. Dr. Yang is currently an Associate Professor with the Department of Energy Technology, Aalborg University. His research focuses on the grid integration of renewable energy, particularly photovoltaic, power converter design, analysis and control, and reliability in power electronics.

Dr. Yang is the Chair of the IEEE Denmark Section. He serves as an Associate Editor of the *CPSS Transactions on Power Electronics and Applications*, the *IET Electronics Letters*, the *IET Renewable Power Generation*, the IEEE JOURNAL OF EMERGING AND SELECTED TOPICS IN POWER ELECTRONICS, and the IEEE TRANSACTIONS ON INDUSTRIAL ELECTRONICS. He was the recipient of the 2018 *IET Renewable Power Generation* Premium Award, and the 2018 *IEEE Transactions on Power Electronics*' Outstanding Reviewers Award.

Frede Blaabjerg (S'86–M'88–SM'97–F'03) was with ABB-Scandia, Randers, Denmark, from 1987 to 1988. From 1988 to 1992, he got the PhD degree in Electrical Engineering at Aalborg University in 1995. He became an Assistant Professor in 1992, an Associate Professor in 1996, and a Full Professor of power electronics and drives in 1998. From 2017 he became a Villum Investigator. He is honoris causa at University Politehnica Timisoara (UPT), Romania and Tallinn Technical University (TTU) in Estonia.

His current research interests include power electronics and its applications such as in wind turbines, PV systems, reliability, harmonics and adjustable speed drives. He has published more than 600 journal papers in the fields of power electronics and its applications. He is the co-author of four monographs and editor of ten books in power electronics and its applications.

He has received 31 IEEE Prize Paper Awards, the IEEE PELS Distinguished Service Award in 2009, the EPE-PEMC Council Award in 2010, the IEEE William E. Newell Power Electronics Award 2014, the Villum Kann Rasmussen Research Award 2014 and the Global Energy Prize in 2019. He was the Editor-in-Chief of the IEEE TRANSACTIONS ON POWER ELECTRONICS from 2006 to 2012. He has been Distinguished Lecturer for the IEEE Power Electronics Society from 2005 to 2007 and for the IEEE Industry Applications Society from 2010 to 2011 as well as 2017 to 2018. In 2019-2020 he serves a President of IEEE Power Electronics Society. He is Vice-President of the Danish Academy of Technical Sciences too.

He is nominated in 2014-2018 by Thomson Reuters to be between the most 250 cited researchers in Engineering in the world..

Shuyong Liu received the B.E. from Huazhong University of Science and Technology in 2000 and Ph.D. degree from Nanyang Technological University in 2008. He is currently with the Electrical Capability Group of Rolls-Royce Singapore. His research interests include the intelligent fault diagnosis of electrical ship power system for unmanned ship, intelligent control system for microgrids.

Gary Wilson is a Principal Technologist with the Electrical Capability Group of Rolls-Royce Singapore. He has worked with the company for 4 years and he leads its research and technology development for marine electrical and control systems. He holds B.Eng. and M.Sc. degrees in Electronics and Electrical Engineering. He started his career in England as a graduate trainee with BAE Systems Submarines before joining Lloyd's Register, where he spent four years developing requirements for its electrical and control systems rules for ships. He then left Lloyd's Register and spent 2.5 years in Perth, Australia, working on mining and oil and gas projects before moving to Singapore. His current research focus includes electrical ship power system design, development of energy storage systems and control and technologies for autonomous systems.